Turbulent coherent structures around an array of blocks

T. Michioka[1]*

1: Dept. of Mechanical Engineering, Kindai University, Japan

* Correspondent author: michioka@mech.kindai.ac.jp

Abstract

To capture the detailed spatial structures of large-scale coherent flow around an array of blocks, proper orthogonal decomposition (POD) is applied to the time-series streamwise and spanwise turbulent velocities obtained by large-eddy simulation. At the first and second POD modes, pairs of the high-velocity structures and low-velocity structures are regularly appeared near the bottom surface at the both sides of the blocks. The structures at the second POD mode are almost identical to those at the first POD mode. The streamwise size of these structures is approximately six times the block height and these structures are strongly linked to the spanwise velocity between the blocks.

Keyword: *Proper Orthogonal decomposition, Large-scale structure, Array of blocks*

1. Background

Investigating large-scale turbulent motions within an idealized urban canopy is crucial for understanding the pollutant removal mechanism from an urban canopy. Michioka et al. (2014) [1], [2] demonstrated that large-scale turbulent motions, accompanying flows across the street between blocks, appear within an idealized urban area. These turbulent motions significantly affect gas dispersion within urban canyons. Similar large-scale turbulent motions have also been observed in flows around an inline array of blocks [3]. However, these studies have not yet extracted the detailed shape of turbulence structures from these complex turbulent flows. Recently, proper orthogonal decomposition (POD) has gained attention as a method for identifying organized turbulence structures within turbulent flows. In this study, POD is applied to instantaneous turbulent flows around an array of blocks to extract large-scale turbulent motions around the array of blocks.

2. Results and discussion

2.1 Large-eddy simulation

The data for the POD was based on the velocity field from a large-eddy simulation around a series of blocks arranged in tandem [3]. A brief overview of the computational domain and conditions is provided here. Figure 1 shows a schematic diagram of the computational domain, with dimensions of 2.4 m × 0.4 m × 0.4 m for the $x \times y \times z$ grid, respectively. The streamwise, spanwise, and vertical directions are the $x-$, $y-$, and $z-$axes, respectively. The twelve cube blocks with a height of H (H = 0.05 m) were arranged in tandem on the bottom surface at equal spacing of H, and were oriented perpendicular to the flow. Large-eddy simulation (LES) with the dynamic Smagorinsky model was implemented. A zero-velocity gradient was applied at the outflow boundary, slip conditions were applied at the upper surface, and non-slip conditions were imposed on the ground and block surfaces. Periodic boundary conditions were applied to both lateral sides of the computational domain. The convection term in the momentum equation was discretised using a second-order central scheme, and all other terms were also estimated using a second-order central scheme. A second-order backward implicit temporal discretization was used for the first time derivative term, and a timestep of 2.5×10^{-4} s. The total number of computational cells was approximately 10.5 million, with the mesh around the blocks being uniformly spaced with a side length of H/40. The grid was geometrically stretched away from the blocks.

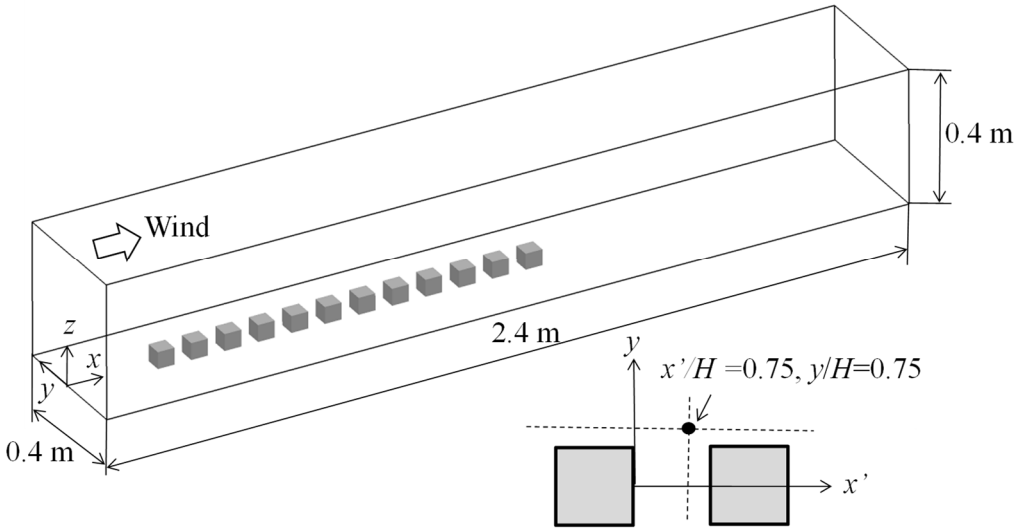

Fig. 1 Schematic diagram of the computational domain

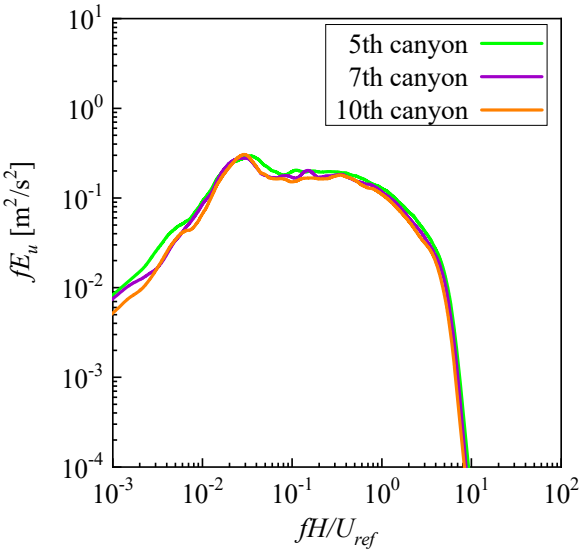

Fig. 2 Energy spectra of the streamwise velocity fluctuations at $x'/H = 0.75$, $y/H = 0.75$ and $z/H = 0.25$.

Figure 2 shows the energy spectra (E_u) of the streamwise velocity fluctuations at $x'/H = 0.75$, $y/H = 0.75$, and $z/H = 0.25$ for 5th, 7th, and 10th canyons. Here, x' represents the streamwise distance from the leeward surface of the windward block, and U_{ref} is the mean streamwise velocity at $z = 2H$. The peak of E_u is observed at $fH/U_{ref} \approx 0.03$ at 5th, 7th, and 10th canyons. This means that large-scale turbulent structures corresponding to $fH/U_{ref} \approx 0.03$ are generated at the side of the block ($y/H = 0.75$).

2.2 Proper orthogonal decomposition

To extract these turbulent structures around the block at $z/H = 0.25$, POD is applied. Snapshots are stored for every 1000 time steps, and time interval is 4.0×10^{-3} s. The snapshots are only stored after the flow fields have become fully develop. To reduce computational costs, snapshot POD is employed. The instantaneous velocity fluctuation can be represented in vector form $u'(t)$ and their collection over time can be arranged in a matrix form,

$$X = [u'(t_1), u'(t_2), \cdots u'(t_m)] \quad \in R^{n \times m}. \tag{1}$$

Here, n represents the number of grid points, and m represents the number of time-series data. The covariance

matrix R of the matrix X is

$$R = XX^T. \tag{2}$$

The eigenvalue problem of R is solved as,

$$RV = \Lambda V. \tag{3}$$

The matrices V and Λ consist of the respective eigenvectors v_j and eigenvalues λ_j. The POD mode is expressed as,

$$\Phi = \mathrm{X}V\Lambda^{-1/2}. \tag{4}$$

The velocity fluctuations in the original field are expressed as a linear combination of the POD mode $\Phi = [\phi_1, \phi_2, \cdots \phi_\mathrm{n}]$ and their corresponding temporal coefficients a_j,

$$u'(x,t) = \sum_j a_j(t)\,\phi_k(x). \tag{5}$$

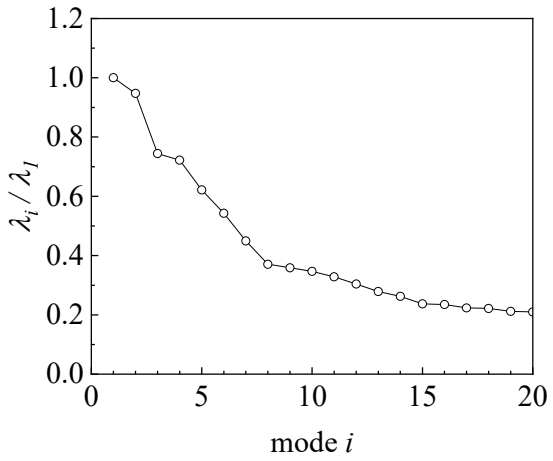

Figure 3 The eigenvalues of each POD mode.

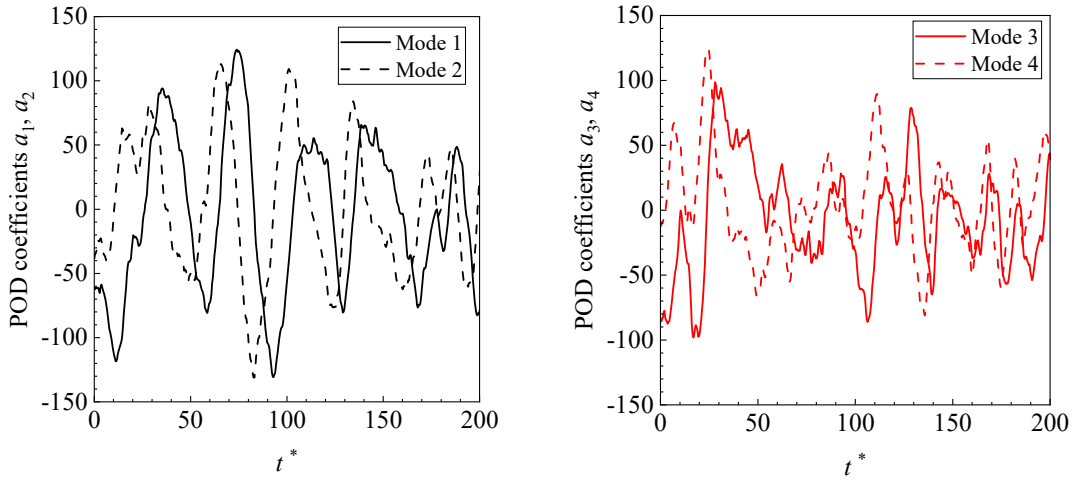

Figure 4 The variation of POD coefficients a_1, a_2 ,a_3 and a_4.

2.3 Eigenvalues and POD coefficients

Figure 3 shows the eigenvalues of each POD mode, with each eigenvalue normalized by the eigenvalues in mode 1. The eigenvalues of the POD modes represent the turbulent energy associated with the corresponding modes. The eigenvalue in mode 1 is nearly identical to that in mode 2. Similarly, the eigenvalue in mode 3 matches that in mode 4. Thus, the POD mode 1 and mode 2 form a pair, and POD mode 3 and mode 4 form another pair. Figure 4 shows the variation of POD coefficients a_1, a_2, a_3 and a_4. The shape of the 1st and 2nd POD coefficients are not exactly sinusoidal, but these shapes roughly resemble a sine function, with different amplitudes. In addition, the 1st and 2nd POD coefficients display the almost same period of $t^* \approx 40$, but they are phase-shifted by about a quarter of wavelength. POD modes 3 and 4 do not exhibit any clear periodic variations.

To investigate which frequency dominates the POD modes, the energy spectra of the POD coefficients is shown in Figure 5. The power spectra for all four modes decrease dramatically at $fH/U_{ref} \approx 0.04$, and the small-scale variance is not represented for the four modes. The power spectra at both mode 1 and 2 have a peak for $fH/U_{ref} \approx 0.02$, which roughly corresponds to that of the energy spectra of the streamwise velocity fluctuations ($fH/U_{ref} \approx 0.03$). This means the 1st and 2nd POD modes represent the almost large-scale structure at $fH/U_{ref} \approx 0.02$. The power spectra at both mode 3 and 4 have almost the same value of around 200 for $fH/U_{ref} < 0.04$. The large-scale structures at the various frequency are represented.

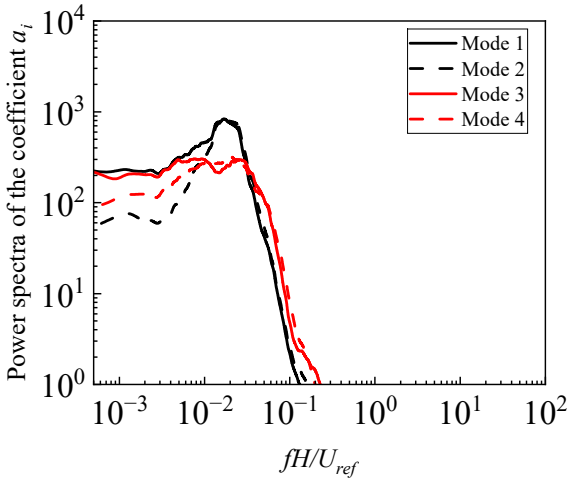

Figure 5 Power spectra of the POD coefficients a_1, a_2 ,a_3 and a_4.

2.4 Spatial structure

Figure 6 shows the spatial structure of top four POD modes of the streamwise velocity fluctuations u' and spanwise velocity fluctuations v' at $z/H = 0.25$. In this figure, red indicates positive values, while blue indicates negative values. The spatial structures of u' for both modes 1 and 2 extend approximately $6H$ in length and are aligned in the downstream direction. The spatial structures in modes 1 and 2 are very similar, with the peak positions shifted by approximately half a wavelength in the streamwise direction. Therefore, modes 1 and 2 are considered nearly paired modes, indicating the presence of periodic spatial structures.

In mode 1, POD structures with a positive value can be observed in the upper area ($y > 0$) of the second to fifth canyons, while those with a negative value appear in the lower area ($y < 0$), with negative spatial structures of v' appearing in the canyons between them. Similarly, in the six to eight canyons, negative turbulent structures of u' appear in the upper area, while positive spatial structures appear in the lower area, with positive spatial structures of v' appearing in the canyons between them. Similar relationships between POD modes are observed in mode 2, indicating the presence of spatial structures of approximately $6H$ in length at the side of the blocks, which are coupled with the flow between the canyons. These spatial structures correspond to the turbulent structures at $fH/U_{ref} \approx 0.03$ in the energy spectrum of u' as shown in Figure 2, and were extracted through POD analysis.

In modes 3 and 4, spatial structures of approximately $6H$ in length are also observed. In mode 4, positive turbulent structures of u' with a length of around $12H$ appear between the second and eight canyons but they

seem to be interrupted around the four and five canyons. This interruption is caused by the presence of positive structures of v' between fourth and fifth canyon, which act to separate the positive turbulent structures of u'. Although large-scale spatial structures larger than $6H$ may develop on the side of the blocks, they do not grow into larger structures as they are not coupled with the flow between the blocks.

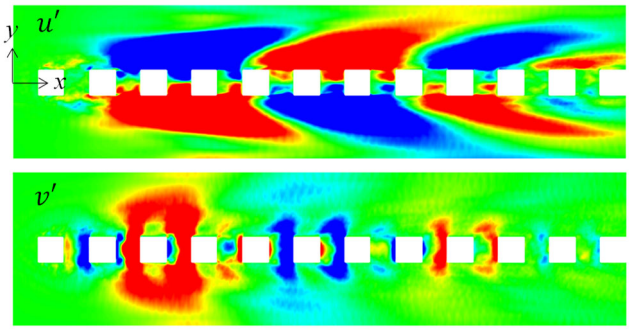

(a) Mode 1

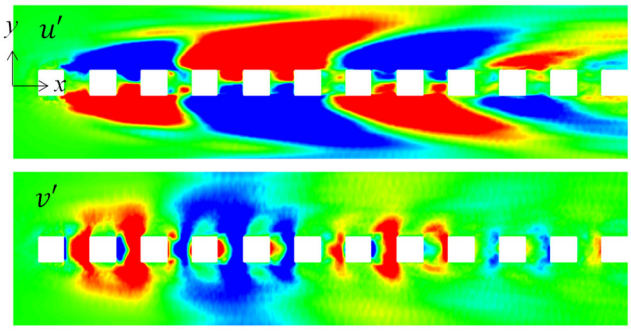

(b) Mode 2

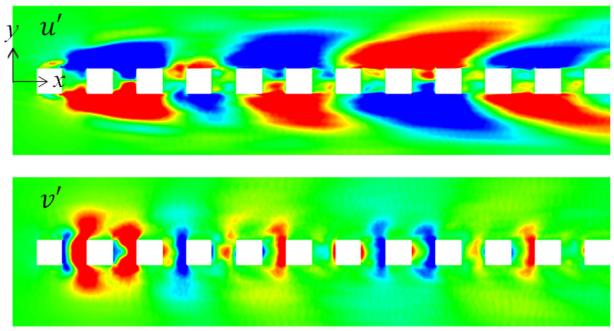

(c) Mode 3

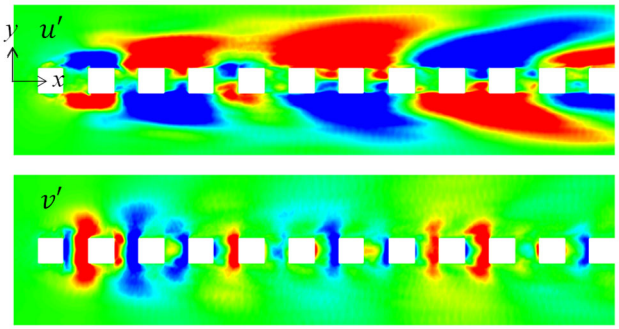

(d) Mode 4

Figure 6 Streamwise velocity fluctuations and spanwise velocity fluctuations of POD modes at $z/H = 0.25$

3. Conclusions

The detailed spatial structures of large-scale coherent flow around an array of blocks are extracted using proper orthogonal decomposition (POD). The turbulent structures with a length approximately six times the block height is appeared near the bottom surfaces. These turbulent structures are coupled with the flow in the spanwise direction between the blocks.

References

[1] Michioka, T., Takimoto, H., Ono, H., and Sato, A., "Effects of Fetch on Turbulent Flow and Pollutant Dispersion within a Cubical Canopy", *Boundary-Layer Meteorology,* Vol.168, (2018), pp. 247-266.

[2] Michioka, T., Takimoto, H. and Sato, A. "Large-Eddy Simulation of Pollutant Removal from a Three-Dimensional Street Canyon", *Boundary-Layer Meteorology*, Vol.150, (2014), pp. 259-275.

[3] Michioka, T., "Turbulent flow around an inline array of blocks", *Environmental Fluid Mechanics*, Vol. 22, (2022), pp. 1005-1024.

Acknowledge

This research was supported by the Japan Society for the Promotion of Science (JSPS), KAKENHI(No. 22K04440).